Asian Journal of Chemistry; Vol. 33, No. 7 (2021), 1563-1572

ASIAN JOURNAL OF CHEMISTRY

https://doi.org/10.14233/ajchem.2021.23217

Fluorescence Recognition of Al(III) Ions by a New Chemosensor Based *E*-4-((1-(10*H*-Phenothiazin-2-yl)ethylidene)amino)-*N*-(pyrimidin-2-yl)benzenesulfonamide

P. Vijayakumar[1], M. Arockia Doss[2], S. Nargis Negar[3] and R. Renganathan[1,*]

[1]School of Chemistry, Bharathidasan University, Tiruchirappalli-620024, India
[2]Department of Chemistry, St. Joseph University, Nagaland-797115, India
[3]Department of Nanoengineering, Center for Physical Sciences and Technology, Savanoriu Ave. 231, LT-02300 Vilnius, Lithuania

*Corresponding author: E-mail: rrengas@gmail.com

Received: 25 March 2021; *Accepted*: 28 April 2021; *Published online*: 26 June 2021; AJC-20398

A novel Schiff base derivative *E*-4-((1-(10*H*-phenothiazin-2-yl) ethylidene)amino)-*N*-(pyrimidin-2-yl)benzenesulfonamide (**BT**) was synthesized and characterized by ^{1}H & ^{13}C NMR, FT-IR and mass spectrometry. Compound **BT** acts as a detector for Al^{3+} in ethanol/water HEPES buffer solution (5 mM, pH 7.4, v/v 1:4) at room temperature. The fluorescence intensity observed at 516 nm was increased due to Al^{3+} ion present with a fluorescence response "turn-on" process, when excited at 290 nm. This shows compound **BT** is coordinated to Al^{3+} ion through the NH group and C=NH of the Schiff base blocking the photoinduced transfer (PET) and chelation induced enhanced fluorescence (CHEF) process, to increase the fluorescence intensity of **BT**. The detection limit of **BT** was in a micro-molar range for Al^{3+} ion, confirming high selectivity and sensitivity of **BT**. The **BT**-Al^{3+} ion binding mode and the recognition mechanism of chemosensor were explored by EDTA titration, Job's plot, Mass and FT-IR analysis. The theoretical support was established by DFT calculations.

Keywords: Benzenesulfonamide, Chemosensor, Photoinduced electron transfer, EDTA, DFT.

INTRODUCTION

The fluorescence chemosensors for the development of recognition of transition metal cations are an important area of research for industrial, biological and environmental purposes [1,2]. Owing to their facile syntheses, high sensitivity and selectivity, flexibility and cost-effectiveness, such fluorescence chemosensors have gained exceptional attention [3,4]. One of the main concerns among researchers is the sensitive and selective detection of metal cations in the production of chemosensors. In general, chemosensors have three components: receptor (capable of guest binding selectivity), spacer (which interfaces receptor and signaling), an active unit (capable of altering its properties during metal complexation). Different chemosensors of polycyclic aromatic hydrocarbons, aromatic ring, thiocarbazole, heterocyclic rings, carbazole and even silatranes are reported [5-7]. Aluminium is the most plentiful metal ingredient and biological non-essential ingredient and too much used in manufacturing and everyday life such as food additives, water treatment devices, packaging products, cosmetics and prescription drugs [8-11]. Compared to other metal ions the highly efficient identification of Al^{3+} ions in aqueous solutions are important due to its strong hydrated ability, lack of spectroscopic characteristics and poor coordination power [12-14]. Due to their high coordination power, excellent photophysical performance and ease of synthesis, Schiff base fluorescent chemosensors have recently attracted a lot of attention [15-17]. Aluminum accumulation in the brain induces neuron degeneration, which is followed by various diseases such as Alzheimer, Parkinson disease, lateral amyotrophic sclerosis, dialysis-induced encephalopathy and also multiple sclerosis [18-21]. Thus it has encouraged ongoing studies on the potentially harmful impact of the atmosphere to enhance effective tools for Al^{3+} identification. These techniques include mass spectrometry, spectrophotometer, electrochemistry, graphite furnace atomic absorption spectrometry, inductively coupled plasma mass spectrometry, voltammetry and liquid chromatography [22-24]. Sensing mechanisms such as fluorescence resonance energy transfer, chelation-induced enhanced fluorescence, intermolecular charge transfer and photoinduced

electron transfer are very relevant in fluorescence chemosensors [25-29]. For several years, the Schiff base compound was used in chemistry [30]. There has been substantial use of non-transition metal complexes [30]. Several complexes of Schiff bases have found interesting uses in materials science [31]. In this case, in turn-on chemosensors, the benzenesulfonamide moieties received considerable attention owing to the formation of excimers and high quantum yield [32,33] due to their ability to show a peculiar shift in their emission wavelengths. Comparison with conventional analytical approaches requires, for example, colorimetric methods that could be accomplished by UV-visible spectra with specific benefits, such as detection and even ease of operation, which could be carried out using on-site tests [34].

Benzenesulfonamide type Schiff base ligand (*E*)-4-((1-(10*H*-phenothiazine-2-yl) ethylidene)amino)-*N*-(pyrimindine-2-yl)benzene sulfonamide (**BT**) was studied in this work. The chemosensor activity for Al^{3+} ions in ethanol/water HEPES buffer (5 mM, pH 7.4, v/v 1:4) solution was demonstrated by the UV-visible and fluorescent spectroscopy at ambient temperature. Complexation of **BT** within the Al^{3+} ion was analyzed by FT-IR and ESI-MS spectroscopy.

EXPERIMENTAL

All the chemicals were purchased commercially and used after purification. Throughout the experiments, only distilled water was used. Solutions of different metal ions salts, such as chloride or nitrate salts of Cr^{3+}, Sn^{2+}, Cu^{2+}, Cd^{2+}, Ti^{3+}, Ca^{2+}, Hg^{2+}, Fe^{3+}, Al^{3+}, Ni^{2+}, Sr^{2+}, Mn^{2+}, Zn^{2+}, Pb^{2+} and Al^{3+} ions were prepared. The FT-IR, ^1H &^{13}C NMR and ESI-MS spectroscopy were used to validate the synthesized compound. An Agilent Carry 630 FT-IR spectrometer was used to test infrared at 4000-400 cm^{-1}. The ^1H & ^{13}C NMR spectra were obtained using a Bruker 400 MHz instrument with TMS as the internal norm and DMSO-d_6 as solvent. At room temperature, fluorescence measurements were taken with a Perkin-Elmer LS45 fluorescence spectrophotometer with a scan rate of 1200 nm.

Synthesis of Schiff base derivative BT: 2-Acetylphenothiazine (0.48 g, 2 mmol) and 4-amino-*N*-(pyrimidin-2-yl)-benzene sulfonamide (0.42 g, 2 mmol) were dissolved in absolute ethanol and refluxed for 24 h at 60 ºC. Then, the reaction was confirmed by TLC plate. This solution mixture was poured in distilled H_2O and light brownish yellow precipitate appeared and then filtered and dried for 2 to 3 days. It was recrystallized from absolute ethanol and finally got the product (**Scheme-I**). Yield: 88%. FT-IR (KBr, ν_{max}, cm^{-1}): (C=N) 1591, (NH) 3345; ^1H NMR (DMSO-d_6, 400 MHz) δ ppm: 8.53 (s, 1H), 8.54 (s, 1H), 8.83 (s, 1H), 7.682-7.661 (d, *J* = 8.4 Hz, 2H), 7.409-7.404 (d, *J* = 2.0 Hz, 2H), 7.389-7.384 (d, *J* = 2.0 Hz, 2H), 7.099-7.039 (*J* = 2.4 Hz, 7H), 6.980-6.961 (d, *J* = 7.6 Hz, 2H), 6.841-6.820 (m, *J* = 8.4 Hz, 4H), 6.723-6.700 (m, *J* = 10.4 Hz, 4H), 6.632-6.610 (2, *J* = 8.0 Hz, 2H). ^{13}C NMR (DMSO-d_6, 100 MHz) δ ppm: 196.88, 158.23, 157.15, 152.98, 141.97, 141.16, 136.06, 129.77, 126.25, 126.11, 124.76, 123.25, 122.52, 122.17, 114.53, 112.62, 112.09, 26.44. m.f.: $C_{27}H_{19}N_5O_5S_2$; ESI-MS (*m/z*): calculated for $[M + H]^+$: 473.16; found: 473.27.

UV-vis and fluorescence analysis: In aqueous water, stock solutions of various metal ions, such as nitrate or chloride salts, were prepared. For spectroscopic tests, a stock solution of **BT** (10 µM) was prepared in aqueous water. The absorption and fluorescence spectra were measured in a quartz cell in an ethanol/water HEPES buffer solution (5 mM, pH 7.4, v/v 1:4) at room temperature using a 5 mL mixed solution of **BT** (10 µM) and metal ion solution with an accurate concentration. Both fluorescence experiments were carried out at a wavelength of 290 nm.

Cell culture: The HepG2 cell lines (NCCS, Pune, India) were grown in DMEM with 10% FBS and antibiotics (streptomycin: 50 µg/mL; penicillin: 100 µg/mL) at 37 ºC, 5% CO_2 incubator and cells were developed at 95%.

Anticancer activity and cell viability assay: The cytotoxicity of **BT** was investigated in HepG2 cell lines using a 3-(4,5-dimethylthiazole-2-yl)-2,5-diphenyl tetrazolium bromide (MTT) assay. Cells were seeded onto a 96-well plate with a cell density per disc of 1.5×10^4 and incubated in a medium containing **BT** for 48 h at various concentrations ranging from 0.0 to 500 µL. For each process, triplicate wells with 100 µL of MTT were used. It was incubated for 4 h at 37 ºC, allowing the MTT reaction and metabolically active cells to form formazan crystals. The MTT medium was carefully removed from the wells. DMSO (100 µL) was added to each well and the dishes were shaken for 10 min to remove intracellular formazan crystals. The absorbance was measured using ELISA at 365 nm. The cells images were studied under a fluorescent microscope. The percentage survival was estimated using the following formula:

$$\text{Survival (\%)} = \frac{\text{Live cell number (test)}}{\text{Live cell number (control)}} \times 100$$

Fluorescence microscopic study: The cells were seeded at a density of 3×10^5 cells per dish in a 35 mm culture dish for *in vitro* fluorescence imaging of **BT**. After completion, 60% confluence for fluorescence microscopy was replaced with aluminum nitrate supplemented with the serum to absorb Al^{3+} ion by 40 h forming cells, **BT** (5.0 M), dissolved in DMSO/

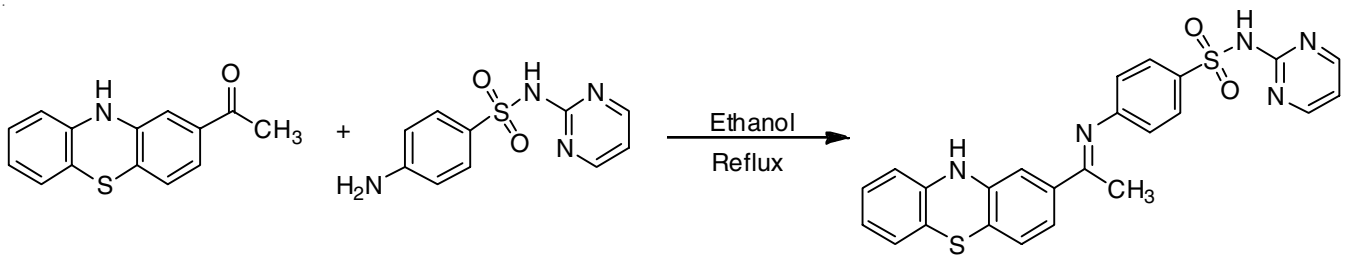

Scheme-I: Synthesis of compound **BT**

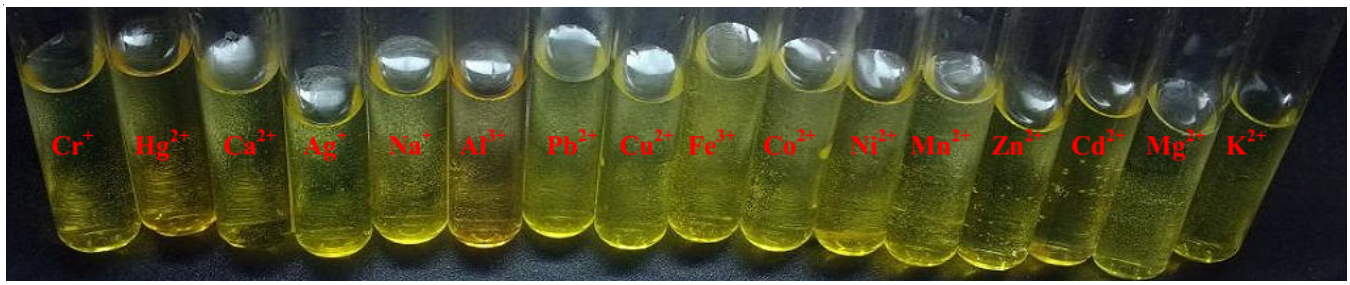

Fig. 1. The colorimetric studies for **BT**

H_2O (99/1), by addition of new media to allow **BT** to be absorbed by cells to form the Al^{3+}-**BT** complex. After that there was a 3 h incubation period. Al^{3+} ions were trypsinized and analyzed for **BT** images at 365 nm using a 10× fluorescent target under a fluorescence microscope. The fluorescence microscope 40x-Olympus FV1000-LX81.z, Camedia software and Adobe Photoshop version 10.0 were used to obtain the bright and fluorescence field information. The Al^{3+} ion was removed from the media for the control trial.

Theoretical studies: The Gaussian09 program [35] was used to perform the computations. The B3LYP method was used to perform the geometry optimization. The molecular electrostatic potentials (MEPs) and Mulliken atomic charges of benzene sulfonamide were plotted in a 3D diagram using optimized structures at the same level theory. Furthermore, the energy gap for benzenesulfonamide was determined using the B3LYP method with a 6-31G (d,p) basis range, as well as HOMO and LUMO energy values. Furthermore, theoretical measurements were used to determine the dipole moment, polarizability and hyper polarizability of molecular polarizabilities.

RESULTS AND DISCUSSION

The fluorescent chemosensor **BT**, *E*-4-(1-(10H-phenothiazin-2-yl)ethylidene)amino)-*N*-(pyrimidin-2-yl)benzenesulfone amide (**BT**) was synthesized (**Scheme-I**) and characterized using FT-IR, ESI-MS, ^1H&^{13}C NMR spectroscopic methods. Colorimetric experiments with naked eye UV-vis and fluorescence spectroscopy in HEPES buffer solution of EtOH:H_2O (1:4 v/v, pH = 7.0) and excitation at 290 nm were also carried out. For different metal ions, the fluorescent chemosensor **BT** solution was investigated and the fluorescence intensity at 516 nm for Al^{3+} ion was investigated further.

Absorption studies: The interaction of analytes with chemosensors was tested using the UV-visible absorption technique [36-39]. At room temperature, experiments were performed in an ethanol/water HEPES buffer (5 mM, pH 7.4, v/v 1:4). Under a UV lamp, the colorimetric tests for **BT** solution showed a bright yellow to medium yellow colour to the naked eye (Fig. 1).

Compound **BT** has three absorption bands with maximum at 252, 272 and 295 nm, which are caused by intra-ligand π→π* electronic transitions and another absorption band at 327 nm, which may be caused by n→π* electronic transitions from non-bonding orbitals on the heteroatoms to π* orbitals of **BT** (Fig. 2). The absorbance of **BT** was explored with different metal ions such as alkali metal ions (Mg^{2+}, Ca^{2+}) and transition metal ions (Cd^{2+}, Cu^{2+}, Ag^{+}, Co^{2+}, Mg^{2+}, Ni^{2+}, Fe^{3+}, Zn^{2+} and Mn^{2+}) in ethanol/water HEPES buffer (5 mM, pH 7.4, v/v 1:4) at ambient temperature. The presence of Al^{3+} ion caused a noticeable shift in wavelength in the absorption spectra of **BT**, while the other metal ions did not cause any significant shifts in the absorption spectrum (Fig. 2). The spectrum of **BT** reveals a new absorption at 415 nm and two new isosbestic points at 308 nm and 340 nm after the addition of Al^{3+} ions (Fig. 3).

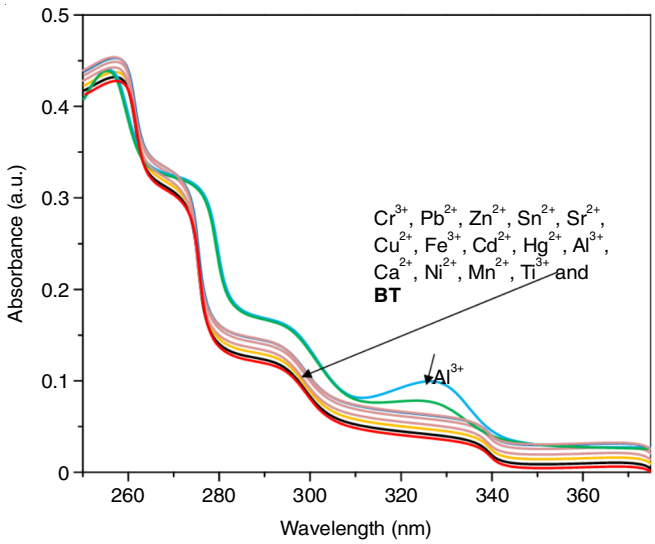

Fig. 2. Absorption spectrum of **BT** (10 μM) with different metal ion (5 equiv.) used in ethanol/water HEPES buffer solution in EtOH:H_2O (5 mM, pH 7.4, v/v 1:4)

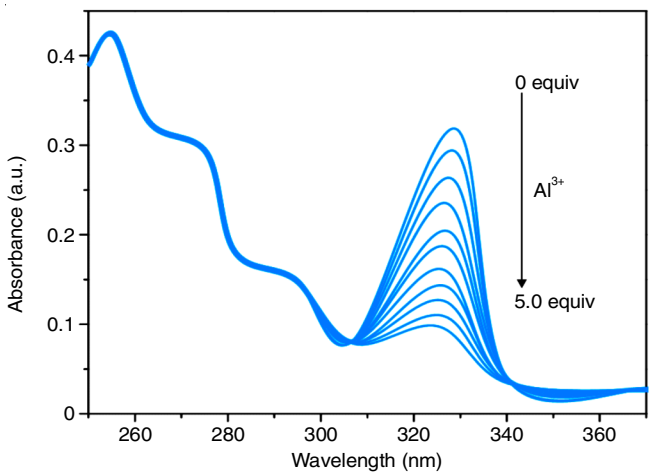

Fig. 3. Absorption spectrum of **BT** (10 μM) with increase concentration of Al^{3+} ion used in ethanol/water HEPES buffer solution (5 mM, pH 7.4, v/v 1:4)

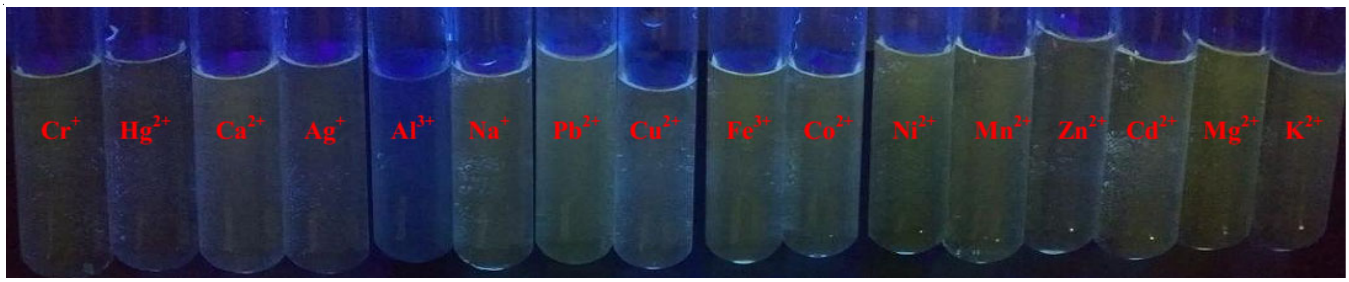

Fig. 4. Fluorometric studies for **BT**

The redshift (bathochromic) in absorption is due to the donor atoms in **BT** binding to Al^{3+} to form a chelate ring, which causes the spectrum to be expanded in conjugation, which may explain the red shift in absorption strength.

Fluorescence studies: The selectivity of **BT** was revealed by pale yellow colour change to blue colour of Al^{3+} because with all metal ions no colour change was observed by fluorescence lamp under 365 nm (Fig. 4).

An equimolar solutions of **BT** (10 µM) was added to solutions of different heavy transition metal ions such as Cr^{3+}, Sn^{2+}, Cu^{2+}, Cd^{2+}, Ti^{3+}, Ca^{2+}, Hg^{2+}, Fe^{3+}, Al^{3+}, Ni^{2+}, Sr^{2+}, Mn^{2+} Zn^{2+}, Pb^{2+} and Al^{3+} ion in ethanol/water HEPES buffer (2 mM 1:4, v/v, pH = 7.0) at ambient temperature. The emission study demonstrated that the compound **BT** shows weak emission maximum intensity at 516 nm observed on excitation at 290 nm (Fig. 5).

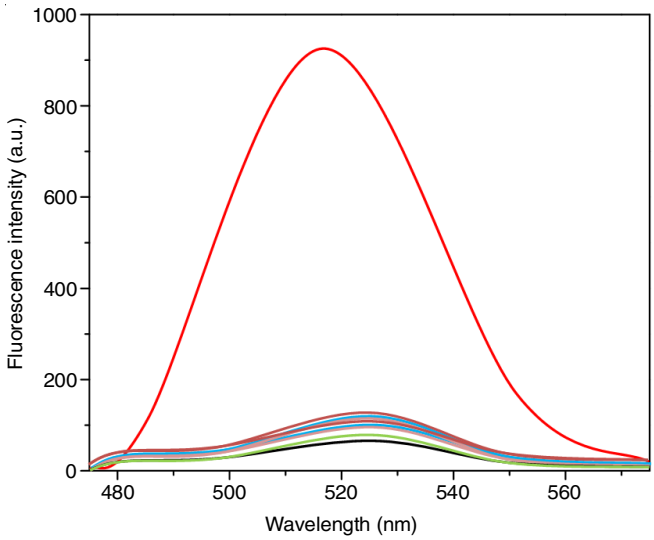

Fig. 5. Fluorescence spectrum of **BT** (10 µM) with different metal ion (5 equiv.) used in ethanol/water HEPES buffer solution in EtOH: H_2O (5 mM, pH 7.4, v/v 1:4)

The emission intensity at 516 nm was red shifted when Al^{3+} ions was added, but no other metal ions made a noticeable difference in the fluorescence spectrum. The switch-ON fluorescence of **BT** caused by metal-ligand binding was fully selective for Al^{3+} ions. Various spectroscopic techniques were used to investigate the binding of the **BT**-Al^{3+} complex. The fluorescence emission intensity at 516 nm gradually decreased with the addition of 2 equiv. of Al^{3+} ion (Fig. 6) becoming stable, reflecting the coordination of **BT** (10 M) with Al^{3+} in stoichiometric complex 1:1 binding mode.

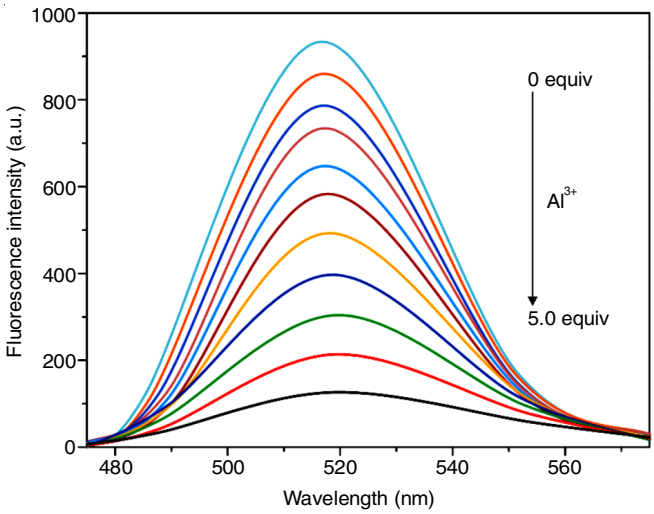

Fig. 6. Fluorescence spectrum **BT** (10 µM) with increase concentration of Al^{3+} ion used in ethanol/water HEPES buffer solution (5 mM, pH 7.4, v/v 1:4)

The complexation of **BT**-Al^{3+} ion was found to be 1:1 stoichiometric using job plots based on fluorescence results (Fig. 7). The binding constant (K) determined from fluorescence intensity at 516 nm using the Benesi-Hildebrand plot was 3.27×10^7 $M^{-1}(Al^{3+})$, indicating that **BT** would bind to Al^{3+} ion (Fig. 8). The detection limit of Al^{3+} ion was calculated using the equation DL = 3/k, where k is the slope of intensity *versus* sample concentration and $R_2 = 0.9965$ is the standard deviation (Fig. 9). Titration of **BT** as a receptor for Al^{3+} ion was carried out to better understand the binding of **BT** as a receptor for Al^{3+} ions.

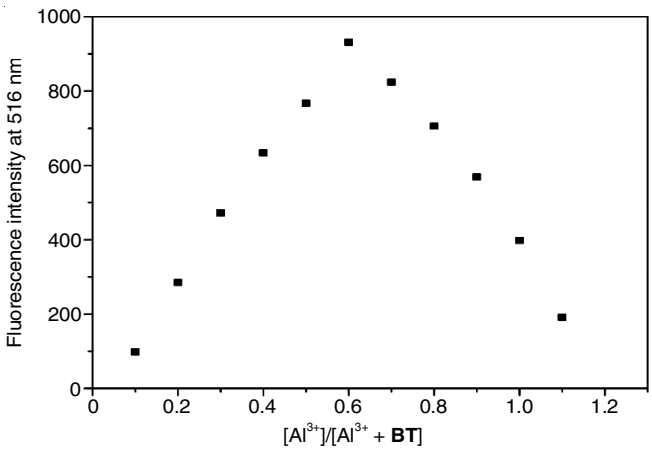

Fig. 7. Job's plot of **BT** + Al^{3+} ion

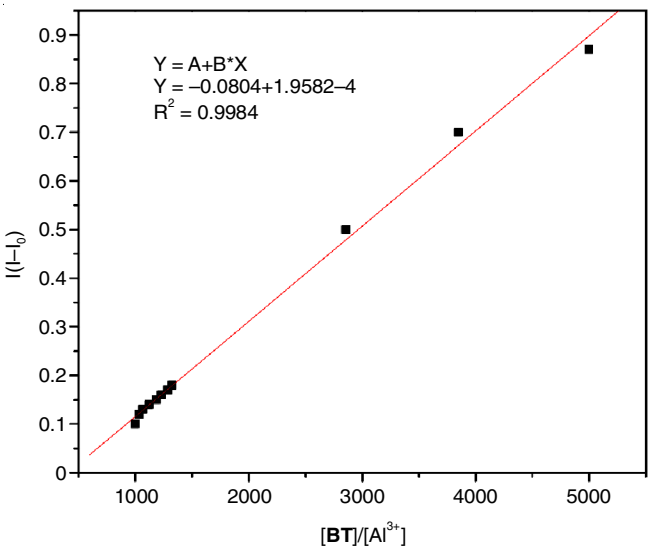

Fig. 8. Benesi-Hildebrand plot from fluorescence titration of **BT** + Al^{3+} ion

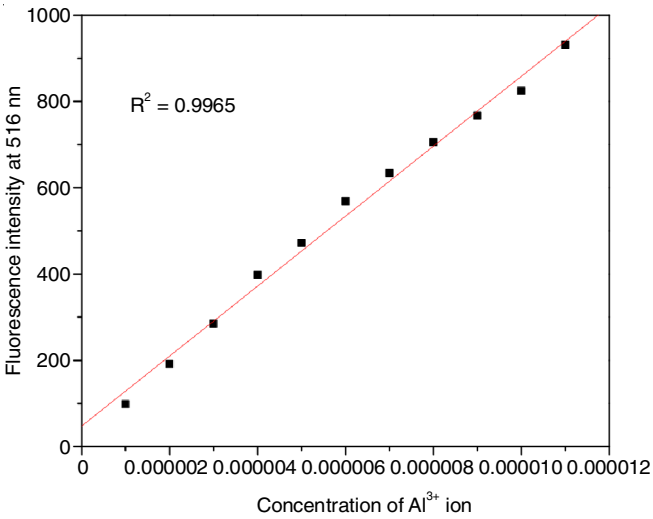

Fig. 9. Determination of limit **BT** (10 μM) with different concentration of Al^{3+} ion

Binding mechanism: Binding studies demonstrate that **BT** is sensitive and selective for Al^{3+} ion as shown by fluorescence changes observed at 516 nm. The inhibition of rotation around the azomethine nitrogen increases the rigidity of the molecular association (CHEF) when Al^{3+} ion is chelated with O and N donors of **BT**. The photoinduced electron transfer (PET) mechanism causes the fluorescence of **BT** to be quenched due to the delocalization of accessible lone pairs of electrons on the imine (C=N) nitrogen atom to the aromatic moiety. Two effects (PET and CHEF), which are responsible for titration processes, were found to increase emission. Further experiments, such as FT-IR and mass spectroscopy, supported the PET process. Due to the addition of 0.5 equiv. of Al^{3+}, the NH stretching peak at 3345 cm^{-1} vanished and a new peak appeared at 3316 cm^{-1}, the functional group of the imine peak at 1591 cm^{-1} vanished and a new peak at 1601 cm^{-1} appeared (Fig. 10). After applying Al^{3+} (1 equiv.) to **BT** solution, the ESI-MS spectrum revealed the exact molecular weight at 498.18 *m/z*, which was compared to the original compound exact mass at

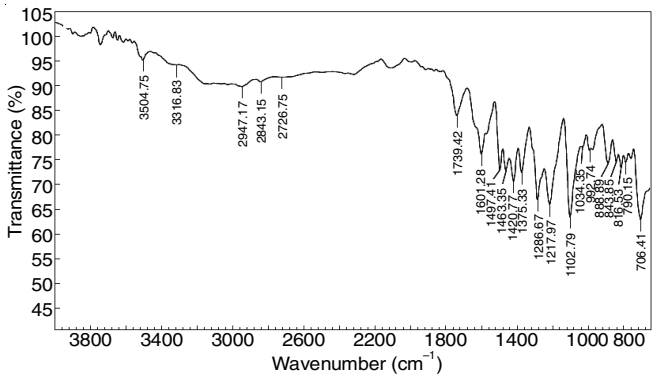

Fig. 10. FT-IR spectrum of **BT** + Al^{3+} ion

473.27 *m/z* (**BT**), confirming the 1:1 stoichiometry for **BT**-Al^{3+} (Fig. 11).

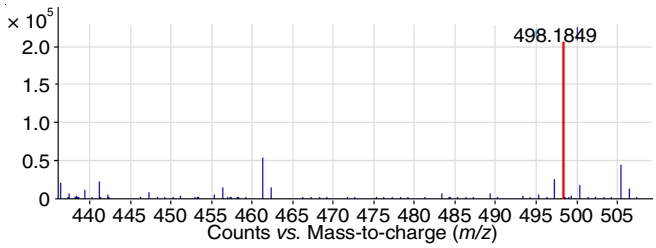

Fig. 11. ESI-MS spectrum of **BT** + Al^{3+} ion

Competitive metal studies: The fluorescence intensity of **BT**-Al^{3+} was examined with other interfering metal ions such as Cr^{3+}, Sn^{2+}, Cu^{2+}, Cd^{2+}, Ti^{3+}, Ca^{2+}, Hg^{2+}, Fe^{3+}, Ni^{2+}, Sr^{2+}, Mn^{2+} Zn^{2+}, Pb^{2+} and Al^{3+} ions in ethanol/water HEPES buffer (5 mM, pH 7.4, v/v 1:4) at ambient temperature. Fig. 12 showed that λ_{ex} wavelength 290 used and λ_{em} intensity at 516 nm was observed.

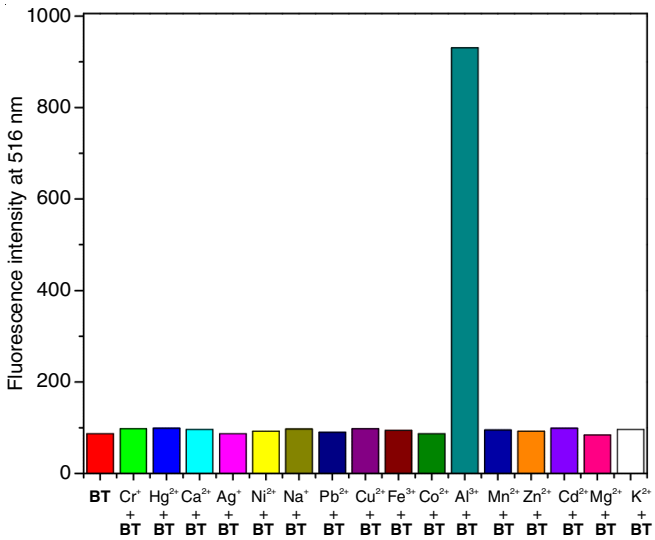

Fig. 12. Emission intensity of **BT** (10 μM) at λ_{em} = 516 nm and the presence of various metal ions (5 equiv.) in ethanol/water HEPES buffer (5 mM, pH 7.4, v/v 1:4) at room temperature

In the presence of Al^{3+} ions (λ_{ex} = 290 nm), the fluorescence intensity of **BT** increased at 516 nm, but other metal ions had no discernible effect on the emission intensity of **BT**

at 516 nm. When **BT** was combined with Al^{3+} ion, the fluorescence intensity at 516 nm (λ_{ex} = 290 nm) was monitored to estimate the main effect of different metal ions (Fig. 13). In the presence of other metal ions, the fluorescence emission strength of **BT** mixed with Al^{3+} did not change significantly. The obtained results show that **BT** can be used to detect Al^{3+} ions in a relatively simple manner.

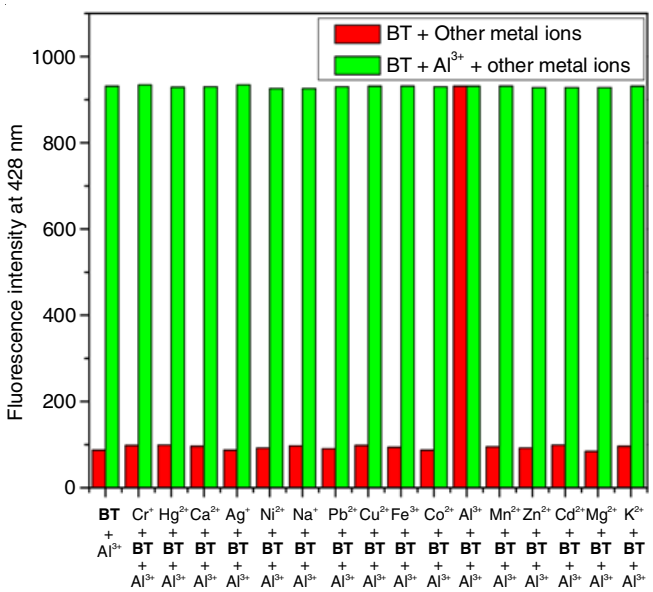

Fig. 13. Competitive metal studies **BT** (10 μM) at λ_{em} = 516 nm and the presence of various metal ions (5 equiv.) in ethanol/water HEPES buffer (5 mM, pH 7.4, v/v 1:4) at room temperature

Reversibility: The probe's reusability is a notable attribute for its use and reversibility tests of **BT** with Al^{3+} ions were performed at room temperature in an ethanol/water HEPES buffer (5 mM, pH 7.4, v/v 1:4) (Fig. 14). The fluorescence spectra of **BT** were observed at 516 nm with 2 equiv. of Al^{3+} ion. After applying a higher concentration of the chelating agent EDTA solution, the emission intensity of metal complexes was decreased, suggesting that the free **BT** was being regenerated. The addition of Al^{3+} ion to the **BT** solution mixture induced fluorescence enhancement within 5 min a second time and the addition of the chelating agent EDTA solution caused fluorescence intensity to be quenched. By gradually adding suitable strong chelating reagents such as EDTA, the obtained results showed that **BT** was a reversible and reusable sensor for Al^{3+} ions for up to three cycles.

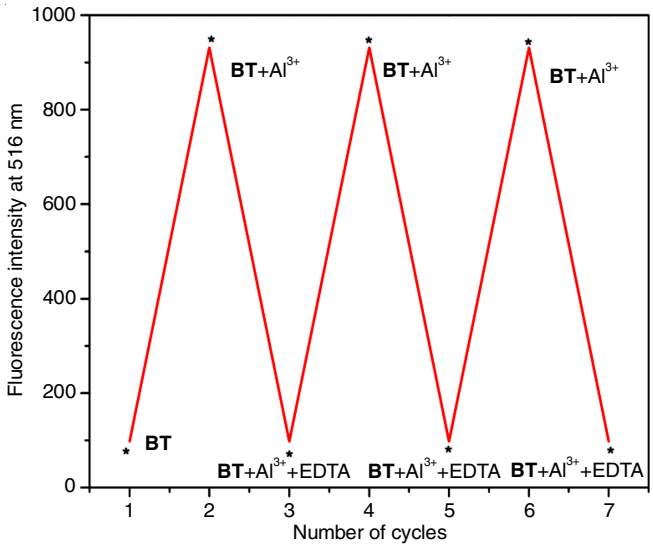

Fig. 14. Emission intensity of **BT** (10 μM) at λ_{em} = 516 nm and the presence of various metal ions (5 equiv.) in ethanol/water HEPES buffer (5 mM, pH 7.4, v/v 1:4) temperature

Cytotoxic activity: The anticancer effects of newly synthesized materials on liver cancer cells (HepG2) were assessed using the MTT-based metabolic assay mentioned previously [40]. The cells (approximately 10,000 cells) were seeded in a well (96-well plate) containing 100 μL of fresh medium and incubated for 24 h. The cells were then treated with 100 μL of various concentrations (ranging from 0.0-500 μM concentration) of the newly generated compound in each well. MTT (100 μL) was applied after 24 h of treatment and incubated for 2-4 h. Then, the reaction was arrested using 100 μL volumes of DMSO and the measurement was carried at 360 nm. The cytotoxicity of active compound was determined by the concentration of extracts that inhibited cell growth by 50% (IC_{50}) as shown in Table-1. The anticancer activity results revealed that the synthesized compound showed potent inhibition of liver cancer cell proliferation.

TABLE-1
IC_{50} VALUES OF **BT** AGAINST HepG2 CELL LINES

Anticancer effect of BT on HepG2 cell line	
Concentration (μM)	Cell viability (%)
0	100
0.9	95
1.9	82
3.9	75
7.8	61
15.6	43
31.25	27
62.5	18
125	11
250	7
500	3

Cell imaging: The HepG2 cancer cells were exposed to compound **BT** for 30 min at 37 ºC after being incubated with Al^{3+} ions (0-100 μg/mL). Because of their high emission intensity in the presence of the probe, compound **BT**-Al^{3+} ions were chosen for the cell imaging procedure. The confocal fluorescence images of HepG2 cell lines after treatment with DAPI, metal salts, probe and its complexes. For Al^{3+} complex, a proportional increase in sensor concentration (0, 20, 50 and 100 μg/mL) follows a proportional relationship with fluorescence intensity. The linking motif within the living cell can be clearly seen in magnified images (Fig. 15). As a result, the receptor **BT** has a strong cell-permeable property and can be used to detect Al^{3+} ions within living cells. Furthermore, when HepG2 cell lines were used instead of HepG2 cells, a similarity in cell imaging was observed (Fig. 15).

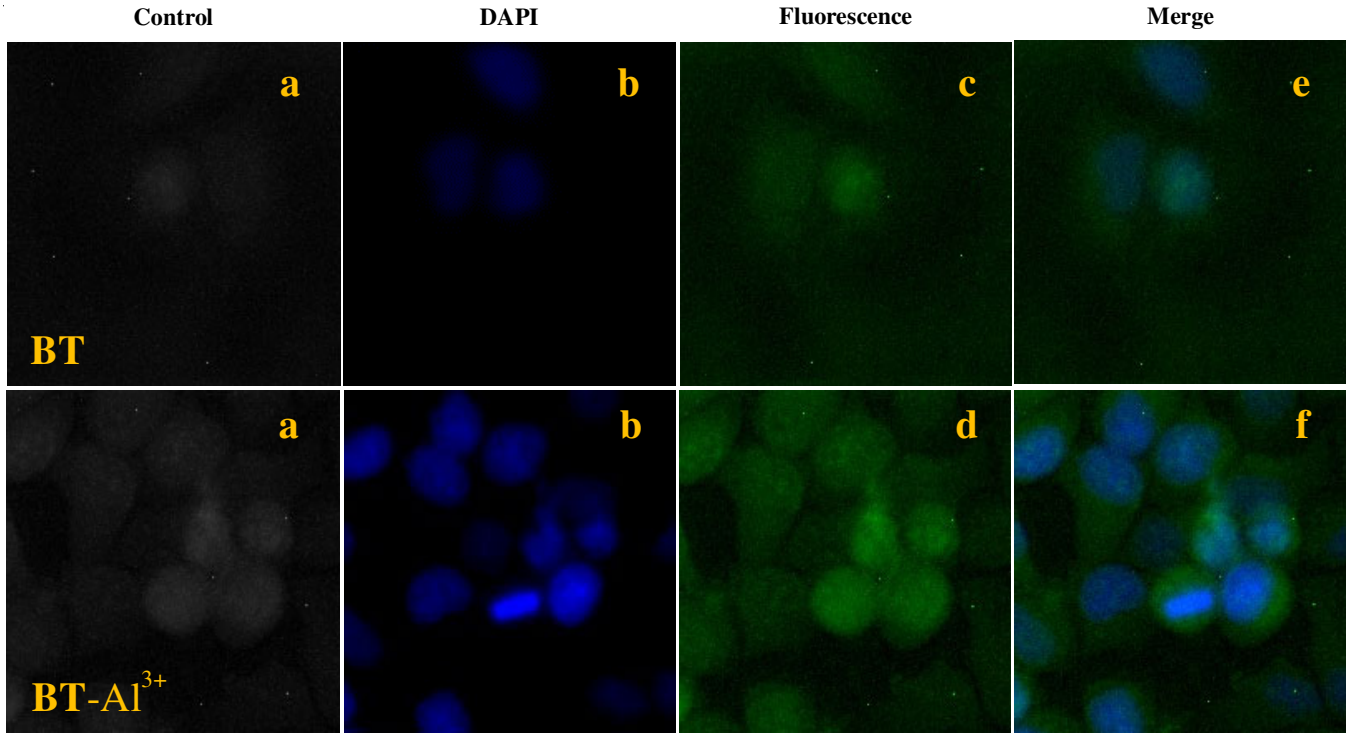

Fig. 15. Confocal fluorescence and merged images of HepG2 cells were stained with DAPI, BT-Al^{3+}, respectively. (a) HepG2 cells incubated with BT-Al^{3+} (5 μM) only, (b) HepG2 cells pre-incubated with BT-Al^{3+} (5 μM) followed by 0.1 mM BT, (c) cells were stained with both DAPI and 5 μM BT-Al^{3+}; (d) cells of (c) further incubated with BT (0.1 mM) for another 30 min, (e) and (f) were merged images. Scale bar, 30 μm

Theoretical studies

HOMO and LUMO analysis: For all the experiments performed on Schiff base compound, the HOMO and LUMO are delocalized from the entire molecule. The energy level of HOMO and LUMO is an extremely important parameter to define the reactivity of molecules because they generally take part in chemical reactions. The lower E_{HOMO} has a weak electron donating capability. However, the higher E_{HOMO} means the good electron donor [41]. In the B3LYP/6-31G(d,p) basis set, the DFT method was used to measure the energy level. The substituted benzenesulfonamide molecules with a methyl group and an NH group in the ring. The largest E_{HOMO} value at 3.24 eV and the lowest E_{LUMO} value at 2.43 eV for compound **BT**, both calculated the band gap energy level at 1.64 eV, because of the decrease in the LUMO value (Fig. 16).

This compound has a stronger electron-donating ability than other Schiff bases. In the meantime, the other calculation method include is dipole moment, polarizability and hyperpolarizability are presented in Table-2. The present work shows the existence of a structure resembling benzenesulfonamide ring increase the HOMO orbitals.

MEP analysis: The MEP is a crucial method for analyzing molecular interactions within a molecule. Hydrogen-bonding reactions, as well as electrophilic and nucleophilic attacking, are extremely helpful in predicting and understanding relevant reactivity sites [42-44]. The optimized structure of molecules at the B3LYP/6-31G(d,p) basis set was used to measure the 3D plot of the MEP diagram for the Schiff molecules (**BT**). Different colours reflected the molecular electrostatic potentials

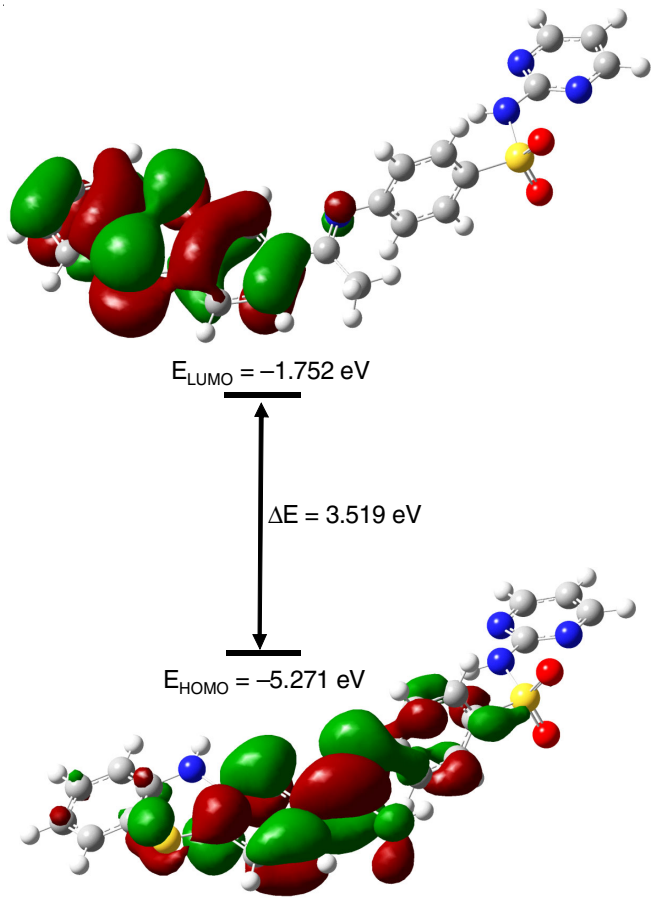

Fig. 16. Energy level diagram of **BT**

TABLE-2
CALCULATED ENERGY VALUES (eV) OF COMPOUND **BT** IN GAS PHASE

B3LYP/6-31G(d,p)	**BT**
E_{HOMO}	-5.2715
E_{LUOMO}	-1.752
$E_{LUMO-HOMO}$	3.5194
Electronegativity	-3.5118
Hardness	1.7595
Electrophilicity index	3.5042
Softness	7.731

at the surface of **BT** molecule. The negative electrostatic potential indicates proton attraction, while the positive electrostatic potential indicates proton repulsion shows in Fig. 17.

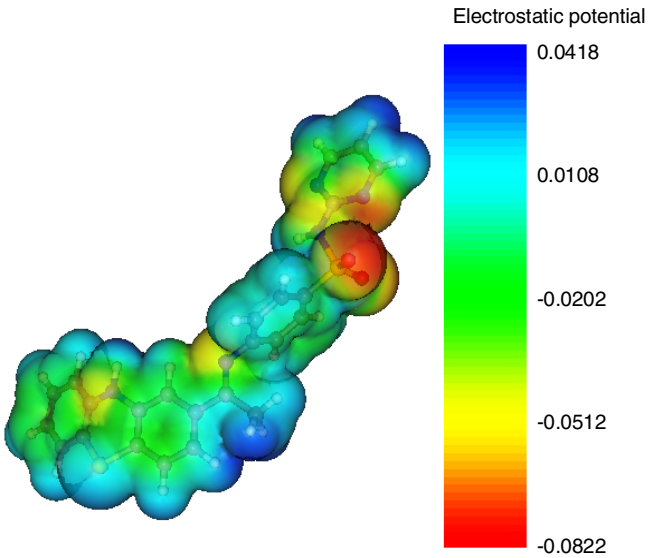

Fig. 17. Molecular electrostatic potential surface of **BT**

Mulliken charge distribution analysis: Mulliken charge population investigation leads to the same conclusion on charge distributions of all Schiff bases of organic compounds. The charge distributions above all atoms propose the formation of donor and acceptor paired relatively the charge transfer in this molecule. The highest negative charge density which is placed on O and N atoms, further responsible for a strong bond between the substrate surface and Schiff base. The Mulliken charge distribution of the molecule is calculated by B3LYP at 6-31G (d,p) level theory. The synthesized compound **BT**, charge distribution shows that all the nitrogen and oxygen highly negative charges and Mulliken charges are very low compared with natural charges (Fig. 18).

Further negative charge could spread all over C1, C3, C5, C6, C8, C11, C15, C18′ and C19′, therefore due to these atoms attached all the molecules. While, other atoms attached to a molecule such as N10, $CH_3$15′, N16, N22, S21, N22, N24 and N24′ are given in Table-3, indicated that compound **BT** can undergo nucleophilic substitution.

NLO Effects: Table-4 shows the approximate hyperpolarizability values for the synthesized compound **BT**. Urea is used as a reference molecule to assess NLO properties and for comparison purposes. Compound **BT** exhibited first hyperpolarizability (β_{tot}) as 139.906×10^{-30} esu, which is six times higher than that of urea (β_0 1.21×10^{-30}). As a result, this molecule may be used as a non-linear optical substance in a future building block.

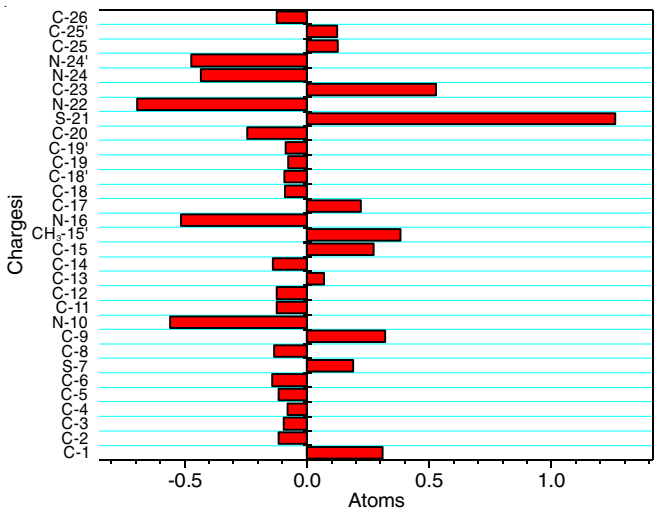

Fig. 18. Mulliken atomic charges for **BT**

TABLE-3
MULLIKEN ATOMIC CHARGES OF COMPOUND **BT**

Atom	BT	Atom	BT
C-1	0.309	N-16	-0.513
C-2	-0.115	C-17	0.22
C-3	-0.094	C-18	-0.089
C-4	-0.078	C-18'	-0.09
C-5	-0.115	C-19	-0.075
C-6	-0.142	C-19'	-0.086
S-7	0.189	C-20	-0.243
C-8	-0.134	S-21	1.259
C-9	0.32	N-22	-0.693
N-10	-0.559	C-23	0.529
C-11	-0.123	N-24	-0.434
C-12	-0.125	N-24'	-0.472
C-13	0.072	C-25	0.125
C-14	-0.139	C-25'	0.122
C-15	0.274	C-26	-0.124
CH_3-15'	0.384		

TABLE-4
DIPOLE MOMENT, POLARIZABILTIY, HYPERPOLARIZABILITY VALUES OF COMPOUND **BT**

Parameter	Dipolemoment (Debye)	Hyperpolarizability (a.u)	
μ_x	9794.942	β_{xxx}	-159.606
μ_y	4546.899	β_{yyy}	4.3205
μ_z	5231.86	β_{zzz}	1.0394
μ_{total}	139.906	β_{xyy}	-47.817
Parameter	Polarisability (a.u)	β_{xxy}	59.3327
α_{xx}	-204.44	β_{xxz}	-68.893
α_{yy}	-175.20	β_{xzz}	108.453
α_{zz}	-183.08	β_{yzz}	-2.432
α_{xy}	-9.77	β_{yyz}	3.7775
α_{xz}	4.56	β_{xyz}	-4.4776
α_{yz}	4.26	β_0 (esu) $\times 10^{-30}$	1.21
α_o (esu) $\times 10^{-23}$	2.8	$\Delta\alpha$ (esu) $\times 10^{-24}$	4.42

Conclusion

In present work, Schiff base derivative was synthesized and characterized by FT-IR, mass and ^{1}H & ^{13}C NMR analysis. The synthesized *E*-4-((1-(10*H*-phenothiazin-2-yl)ethylidene)-amino)-*N*-(pyrimindin-2-yl)benzenesulfonamide (**BT**) exhibited recognition for Al^{3+} in ethanol/water HEPES buffer solution (5 mM, pH 7.4, v/v 1:4) at ambient temperature in a UV-visible and fluorescence spectroscopy. The fluorescence λ_{em} intensity at 516 nm (λ_{ex} wavelength at 290 nm), fluorescence "turn-on" due to the presence of Al^{3+} ion with a high peak below all metal ions. The PET and stimulating CHEF process for **BT**+Al^{3+} ion was coordinated through the NH group and imine nitrogen inhibited and blocked. Job's plot was shown by 1:1 stoichiometric for **BT**-Al^{3+} ion. The binding constant (K) was determined as 3.27×10^{7} M^{-1} (Al^{3+}), the limit of detection **BT** for Al^{3+} ion was observed $R^2 = 0.9965$. Competitive metal ions extensively studied for the presence of Al^{3+} ion, whereas, after the EDTA solution added into **BT**+Al^{3+} ion proved to be reversible and irreversible. The theoretical calculation used in Gaussian 09 program was followed by the B3LYP/6-31G(d,p) basis set.

ACKNOWLEDGEMENTS

One of the authors (PV) thanks to UGC for providing the fellowship (F.4-1/2006(BSR)/7-22/2007(BSR) dated 02.01.2013). Another author (RR) thanks DST Nanomission (SR/NM/NS/1256/2013) and UGC (UGC-2013-35169/2015) for sanctioning the project and Emeritus Fellowship (F.66/2016-17/EMERITUS-2015-17-OBC7855/(SA-II)).

CONFLICT OF INTEREST

The authors declare that there is no conflict of interests regarding the publication of this article.

REFERENCES

1. D. Wu, A.C. Sedgwick, T. Gunnlaugsson, E.U. Akkaya, J. Yoon and T.D. James, *Chem. Soc. Rev.*, **46**, 7105 (2017); https://doi.org/101039/C7CS00240H
2. D. Udhayakumari and V. Inbaraj, *J. Fluoresc.*, **30**, 1203 (2020); https://doi.org/10.1007/s10895-020-02570-7
3. Y.M. Yang, Q. Zhao, W. Feng and F.Y. Li, *Chem. Rev.*, **113**, 192 (2013); https://doi.org/10.1021/cr2004103
4. D.C.E. Persch, D.C.O. Dumele and F. Diederich, *Angew. Chem. Int. Ed.*, **54**, 3290 (2015); https://doi.org/10.1002/anie.201408487
5. G. Singh, A. Singh, P. Satija, G. Sharma, J. Shilpy, J. Singh, J. Singh, K.N. Singh and A. Kaur, *New J. Chem.*, **43**, 5525 (2019); https://doi.org/10.1039/C9NJ00288J
6. G. Singh, J. Singh, S.S. Mangat, J. Singh and S. Rani, *RSC Adv.*, **5**, 12644 (2015); https://doi.org/10.1039/C4RA14329A
7. G. Singh, S. Rani, A. Saroa, S. Girdhar, J. Singh, A. Arora, D. Aulakh and M. Wriedt, *RSC Adv.*, **5**, 65963 (2015); https://doi.org/10.1039/C5RA09004K
8. B. Naskar, R. Modak, Y. Sikdar, D.K. Maiti, A. Bauzá, A. Frontera, A. Katarkar, K. Chaudhuri and S. Goswami, *Sens. Actuators B Chem.*, **239**, 1194 (2017); https://doi.org/10.1016/j.snb.2016.08.148
9. K. Boonkitpatarakul, J. Wang, N. Niamnont, B. Liu, L. Mcdonald, Y. Pang and M. Sukwattanasinitt, *ACS Sens.*, **1**, 144 (2016); https://doi.org/10.1021/acssensors.5b00136
10. S. Gui, Y. Huang, F. Hu, Y. Jin, G. Zhang, L. Yan, D. Zhang and R. Zhao, *Anal. Chem.*, **87**, 1470 (2015); https://doi.org/10.1021/ac504153c
11. E. Yildiz, S. Saçmaci, M. Saçmaci and A. Ülgen, *Food Chem.*, **237**, 942 (2017); https://doi.org/10.1016/j.foodchem.2017.06.055
12. K.S. Ku, P. Muthukumar, S. Angupillai and Y.A. Son, *Sens. Actuators B Chem.*, **236**, 184 (2016); https://doi.org/10.1016/j.snb.2016.05.143
13. L. Tang, S. Ding, K. Zhong, S. Hou, Y. Bian and X. Yan, *Spectrochim. Acta A*, **174**, 70 (2017); https://doi.org/10.1016/j.saa.2016.11.026
14. Z. Li, W. Chen, L. Dong, Y. Song, R. Li, Q. Li, D. Qu, H. Zhang, Q. Yang and Y. Li, *New J. Chem.*, **44**, 3261 (2020); https://doi.org/10.1039/C9NJ06309A
15. S. Wang, G. Men, L. Zhao, Q. Hou and S. Jiang, *Sens. Actuators B Chem.*, **145**, 826 (2010); https://doi.org/10.1016/j.snb.2010.01.060
16. H.Y. Jeong, S.Y. Lee, J. Han, M.H. Lim and C. Kim, *Tetrahedron*, **73**, 2690 (2017); https://doi.org/10.1016/j.tet.2017.03.069
17. Y. Xu, L. Yang, H. Wang, Y. Zhang, X. Yang, M. Pei and G. Zhang, *J. Photoch. Photobio. A.*, **391**, 112372 (2020); https://doi.org/10.1016/j.jphotochem.2020.112372
18. J.A. Edwardson, J.M. Candy, P.G. Ince, F.K. McArthur, C.M. Morris, A.E. Oakley, G.A. Taylor and E. Bjertness, *Ciba Found. Symp.*, **169**, 165 (1992).
19. M. Kawahara, *J. Alzheimers Dis.*, **8**, 171 (2005); https://doi.org/10.3233/JAD-2005-8210
20. J. Savory, M.M. Herman, C.D. Katsetos and M.R. Wills, in Eds.: M. Nicolini, P.F. Zatta and B. Corain, Aluminum in Chemistry Biology and Medicine, Cortina International/Raven Press: Verona, New York, p. 45 (1991).
21. C. Exley, G. Mamutse, O. Korchazhkina, E. Pye, S. Strekopytov, A. Polwart and C. Hawkins, *Mult. Scler.*, **12**, 533 (2006); https://doi.org/10.1177/1352458506071323
22. S. Mondal, A.K. Bhanja, D. Ojha, T.K. Mondal, D. Chattopadhyay and C. Sinha, *RSC Adv.*, **5**, 73626 (2015); https://doi.org/10.1039/C5RA11548E
23. S.Y. Li, D.B. Zhang, J.Y. Wang, R.M. Lu, C.H. Zheng and S.Z. Pu, *Sens. Actuators B Chem.*, **245**, 263 (2017); https://doi.org/10.1016/j.snb.2017.01.149
24. G. Bartwal, K. Aggarwal and J.M. Khurana, *New J. Chem.*, **42**, 2224 (2018); https://doi.org/10.1039/C7NJ04194B
25. S.K. Sahoo, G.D. Kim and H.J. Choi, *J. Photochem. Photobiol. Chem.*, **27**, 30 (2016); https://doi.org/10.1016/j.jphotochemrev.2016.04.004
26. Y. Dong, R. Fan, W. Chen, P. Wang and Y. Yang, *Dalton Trans.*, **46**, 6769 (2017); https://doi.org/10.1039/C7DT00956A
27. K.P. Carter, A.M. Young and A.E. Palmer, *Chem. Rev.*, **114**, 4564 (2014); https://doi.org/10.1021/cr400546e
28. W.N. Lipscomb and N. Sträter, *Chem. Rev.*, **96**, 2375 (1996); https://doi.org/10.1021/cr950042j
29. A.K. Bhanja, C. Patra, S. Mondal, D. Ojha, D. Chattopadhyay and C. Sinha, *RSC Advances*, **5**, 48997 (2015); https://doi.org/10.1039/C5RA06193H
30. K. Zhang, L. Zhang, S. Zhang, Y. Hu, Y. Zheng and W. Huang, *Inorg. Chem.*, **54**, 5295 (2015); https://doi.org/10.1021/acs.inorgchem.5b00283
31. X. Liu and J.-R. Hamon, *Coord. Chem. Rev.*, **389**, 94 (2019); https://doi.org/10.1016/j.ccr.2019.03.010
32. T. Simon, M. Shellaiah, V. Srinivasadesikan, C.-C. Lin, F.-H. Ko, K.W. Sun and M.-C. Lin, *Sens. Actuators B Chem.*, **231**, 18 (2016); https://doi.org/10.1016/j.snb.2016.02.136
33. A. Singh, R. Singh, M. Shellaiah, E.C. Prakash, H.-C. Chang, P. Raghunath, M.-C. Lin and H.-C. Lin, *Sens. Actuators B Chem.*, **207**, 338 (2015); https://doi.org/10.1016/j.snb.2014.09.105

34. J. Wan, K. Zhang, C. Li, Y. Li and S. Niu, *Sens. Actuators B Chem.*, **246**, 696 (2017); https://doi.org/10.1016/j.snb.2017.02.126
35. M.J. Frisch, G.W. Trucks, H.B. Schlegel, G.E. Scuseria, M.A. Robb, J.R. Cheeseman, G. Scalmani, V. Barone, B. Mennucci, G.A. Petersson, H. Nakatsuji, M. Caricato, X. Li, H.P. Hratchian, A.F. Izmaylov, J. Bloino, G. Zheng, J.L. Sonnenberg, M. Hada, M. Ehara, K. Toyota, R. Fukuda, J. Hasegawa, M. Ishida, T. Nakajima, Y. Honda, O. Kitao, H. Nakai, T. Vreven, J.A. Montgomery Jr., J.E. Peralta, F. Ogliaro, M. Bearpark, J.J. Heyd, E. Brothers, K.N. Kudin, V.N. Staroverov, T. Keith, R. Kobayashi, J. Normand, K. Raghavachari, A. Rendell, J.C. Burant, S.S. Iyengar, J. Tomasi, M. Cossi, N. Rega, J.M. Millam, M. Klene, J. E. Knox, J.B. Cross, V. Bakken, C. Adamo, J. Jaramillo, R. Gomperts, R.E. Stratmann, O. Yazyev, A.J. Austin, R. Cammi, C. Pomelli, J.W. Ochterski, R.L. Martin, K. Morokuma, V.G. Zakrzewski, G.A. Voth, P. Salvador, J.J. Dannenberg, S. Dapprich, A.D. Daniels, O. Farkas, J.B. Foresman, J.V. Ortiz, J. Cioslowski and D.J. Fox, GAUSSIAN 09, revision B.01.; Gaussian Inc.: Wallingford, CT (2010).
36. Z. Wang, N. Wang, X. Han, R. Wang and J. Chang, *J. Biomol. Struct. Dyn.*, **36**, 3388 (2018); https://doi.org/10.1080/07391102.2017.1388287
37. Z. Li, Z. Wang, N. Wang, X. Han, W. Yu, R. Wang and J. Chang, *J. Pharm. Biomed. Anal.*, **149**, 290 (2018); https://doi.org/10.1016/j.jpba.2017.11.007
38. T. Ren, Z. Wang, L. Zhang, N. Wang, X. Han, R. Wang and J. Chang, *J. Fluoresc.*, **27**, 1467 (2017); https://doi.org/10.1007/s10895-017-2086-2
39. L. Zhang, T. Ren, X. Tian, Z. Wang, W. Yu, R. Wang and J. Chang, *J. Fluoresc.*, **27**, 369 (2017); https://doi.org/10.1007/s10895-016-1965-2
40. T. Mosmann, *J. Immunol. Methods*, **65**, 55 (1983); https://doi.org/10.1016/0022-1759(83)90303-4
41. S. Antonczak, *J. Mol. Struct.*, **856**, 38 (2008); https://doi.org/10.1016/j.theochem.2008.01.014
42. I. Lukovits, E. K'alm'an and F. Zucchi, *Corrosion*, **57**, 3 (2001); https://doi.org/10.5006/1.3290328
43. E. Scrocco and J. Tomasi, *Adv. Quantum Chem.*, **11**, 115 (1978); https://doi.org/10.1016/S0065-3276(08)60236-1
44. V. Arjunan, P.S. Balamourougane, C.V. Mythili, S. Mohan and V. Nandhakumar, *J. Mol. Struct.*, **1006**, 247 (2011); https://doi.org/10.1016/j.molstruc.2011.09.015